

# Learning a Stochastic Differential Equation Model of Tropical Cyclone Intensification from Reanalysis and Observational Data

Kenneth Gee<sup>1</sup> and Sai Ravela<sup>1</sup>

<sup>1</sup>Earth Signals and Systems Group, Massachusetts Institute of Technology, Cambridge, MA 02139, USA

January 14, 2026

## Abstract

Tropical cyclones are dangerous natural hazards, but their hazard is challenging to quantify directly from historical datasets due to limited dataset size and quality. Models of cyclone intensification fill this data gap by simulating huge ensembles of synthetic hurricanes based on estimates of the storm's large scale environment. Both physics-based and statistical/ML intensification models have been developed to tackle this problem, but an open question is: can a physically reasonable and simple physics-style differential equation model of intensification be learned from data? In this paper, we answer this question in the affirmative by presenting a 10-term cubic stochastic differential equation model of Tropical Cyclone intensification. The model depends on a well-vetted suite of engineered environmental features known to drive intensification and is trained using a high quality dataset of hurricane intensity (IBTrACS) with estimates of the cyclone's large scale environment from a data-assimilated simulation (ERA5 reanalysis), restricted to the Northern Hemisphere. The model generates synthetic intensity series which capture many aspects of historical intensification statistics and hazard estimates in the Northern Hemisphere. Our results show promise that interpretable, physics style models of complex earth system dynamics can be learned using automated system identification techniques.

# 1 Introduction

Tropical Cyclones (TCs) are among the costliest and deadliest natural disasters [38, 41]. To plan for and mitigate the risk posed to coastal communities by TCs, it is important to estimate their intensity at landfall. Storm return periods and intensity distributions at landfall are common metrics of hazard, but the return periods of the most intense storms exceed the duration of high quality intensity observations ( $\sim 40$  years [26]) which limit the strength of such estimates from historical data alone [40].

One way to fill this data gap is to use models to simulate a large collection of realistic TC tracks and intensities. Tropical cyclones emerge in Global Circulation Models, so one might be tempted to run GCMs for a long time and extract storm data. However, this approach is computationally infeasible as GCMs at the resolution to resolve TCs are prohibitively expensive [1]. Sacrificing resolution for computational speed also fails because the dynamics of the inner eyewall are crucial for intensification [49] but requires kilometer-scale resolution - the Integrated Forecasting System (IFS) run at  $1/4^\circ$  resolution [11] systemically underestimates intensity for this reason [21]. However, intensification is driven in large part by the large-scale environment surrounding a storm [17], enabling the development of inexpensive models of intensity which depend only on coarse-grained features of the environment [13] which still accurately capture the statistics of intensity. Coupled with separate track generation and cyclogenesis models, “downscaling” models of tropical cyclones have been developed [31, 28, 4] which generate completely synthetic storms. They have been used to generate a dataset of 10,000 years of storms [4] in present climate for TC hazard estimation, and to generate TC hazard estimates in future climate scenarios where no data is available [32].

The intensity, track and genesis components have all developed appreciably over recent decades, but intensification remains the most challenging because it depends on several nonlinear and challenging to parameterize processes [16]. The intensity, here measured as the maximum sustained azimuthal wind speed, is nonlinear because it depends on a positive feedback between surface wind speed and enthalpy extraction from the surface [18], and the parameterization of this exchange depends on challenging-to-constrain details of sea spray in high winds [15]. Further, the impact of synoptic vertical wind shear on intensity depends on parameterizations of turbulent downdrafting of low-entropy environmental air into the boundary layer [46].

What, then, is the best way to model intensification? Many approaches have been developed to answer this question. Several authors have trained autoregressive models of intensity, which are linear models that forecast

intensity at discrete increments of time as a function of lags of intensity and large-scale environmental variables [29, 4, 10]. Such models often match the statistics of observed tracks closely but can generalize poorly in regions with little training data [35]. StormCast is a machine learning emulator of a Convection Allowing Model (CAM) of atmospheric dynamics which can rapidly generate detailed cyclone dynamics (including genesis, track and intensity at once) [39], but such models may also struggle to generalize to out-of-training data atmospheric states such as those from future climate scenarios, and StormCast doesn't couple to the underlying ocean which is a key driver of intensity [43]. Finally, physical models have been developed, such as the Coupled Hurricane Intensity Prediction System (CHIPS) [17] which couples an intensity model to a simplified 1d model of the upper ocean, and FAST [12] which is an Ordinary Differential Equation model arrived at empirically to inexpensively emulate CHIPS. Both models were developed using physical understanding and hence are expected to generalize well. They can also be used to deepen understanding of TC intensification dynamics through a nonlinear dynamics analysis [45], but exhibit biases such as underestimation of extreme intensities [31].

An approach which has not been attempted is to learn a physics-style model, such as an ordinary differential equation (ODE) or stochastic differential equation (SDE), from observational cyclone intensity and reanalysis data directly. Such a model would be amenable to mathematical analysis and would fit well to data by construction. A wealth of literature has developed methodologies to learn such models. The Nonlinear Autoregressive Moving Average model with Exogenous inputs (NARMAX) paradigm [22] refers to a large body of techniques for learning nonlinear autoregressive and nonlinear continuous models using time series data. More recently, interest has been rekindled with the Sparse Identification of Nonlinear Dynamical systems (SINDy) framework [5] which regresses finite-difference quotient estimates of the system's derivative onto a large library of candidate features. Model structure is learned by imposing a sparsity constraint on regression so that only a small subset of the initial feature library are ultimately utilized. SINDy, however, is not well-suited to the intensification problem because observations of TC intensity are discretized to 5 knot bins and available at coarse temporal resolution of 6h, making finite-difference quotient intensity estimates very noisy. Integral SINDy instead uses integrations of the underlying differential equation to construct a sparse linear regression problem which is more robust to observation noise [44, 37]. However, this approach suffers from performing quadrature at the resolution of observations which compromises integration quality in temporally coarse settings. The Informative Ensemble Kalman Learner (IEKL) is another approach to system identification which instead integrates ODEs at arbitrary numerical precision and uses observations whenever they are available to

perform parameter estimation and structure learning [48]. Given its numerical flexibility, the IEKL has the potential to recover dynamical systems in a wider range of cases than previous approaches.

In this paper, we show that nonlinear system identification techniques can learn a physics-style model of intensity from observational data and simulations. We present a 10-term polynomial stochastic differential equation of intensity which depends on estimates of the large scale environment surrounding the storm. The model was learned directly from a synthesis of high-resolution simulations and observations, specifically the reanalysis climate model ECMWF Reanalysis 5 (ERA5) [19] and the observational dataset of hurricane intensity International Best Track Archive for Climate Stewardship (IBTrACS) [26]. Methodologically, we solve an Integral SINDy problem then fine tune parameters using the inference stage of the IEKL. The model produces intensity time series which match many aspects of the statistics of observed storms. The model is interpretable in the context of existing theoretical understanding of TC intensification and produces reasonable estimates of TC return periods and landfalling intensity distribution. While these results depend on pre-engineered features, they demonstrate promise that such system identification methods can accelerate the scientific process of identifying low order models of complex earth system dynamics.

In Section 2, we review the environmental variables which drive the intensification model and introduce the equation structure. In Section 3, we present the learned equation, analyze its bifurcations, and compare the climatology and individual intensification time series with those from the historical record. In Section 4, we detail the model training procedure and sparsity promotion step. In Section 5, we discuss our results and point to future directions.

## 2 Intensification Features

The model depends on a set of environmental features that are known to drive TC intensification. These features are already “engineered” based on previous scientific effort and are not inferred from primitive variables. Each feature is estimated from ERA5 reanalysis and forces intensification along a track.

The first feature is the Potential Intensity  $V_p$ , a maximum possible intensity given the vertical temperature profile surrounding the storm [3]. A Tropical Cyclone converts thermal energy from the warm sea surface to kinetic energy by releasing the heat into the cool upper atmosphere. A thermodynamic argument constrains the maximum possible kinetic energy using the temperature profile of the air column. A cyclone is often thought of as approaching its potential intensity, but its ability to achieve this maximum is bounded by other processes.

The second feature captures the impact of the upper ocean on TC intensity. Tropical cyclone winds stir up the underlying ocean and upwell cold waters from below the mixed layer. This cools the sea surface and cuts off the storm's energy source, damping the cyclone. This effect is strongest with a shallow mixed layer  $h_m$ , steep sub-mixed layer stratification  $\Gamma$ , and a slow cyclone velocity (not wind speed)  $u_T$ , and strong intensity  $v$ .

An estimate of the climatological upper ocean heat content as a function of the track and environment is given by

$$z = 0.01\Gamma^{-0.4}h_m u_T V_p^{-1} \quad (1)$$

which takes positive values and is treated as dimensionless [43]. The impact of intensity  $v$  is incorporated in another nondimensional parameter

$$\alpha = 1 - 0.87 \exp(-z/v) \quad (2)$$

which is bounded to  $\alpha \in [0.13, 1]$  and where zero damping corresponds to unity [43]. Only  $\alpha$  is used directly in the model,  $z$  is an internal variable in the computation of  $\alpha$ .

The third feature is the environmental mid-level entropy deficit  $\chi$ , which measures the degree to which the air surrounding the cyclone is cooler and drier than that in its inner core. More specifically, it measures the difference in entropy at 600hPa between the cyclone's inner core and surrounding environment [47]. High values indicate that intruding air from the environment will dry out the inner core which limits moist convection and damps intensity.

The final physical variable is synoptic vertical wind shear  $S$ . Synoptic wind shear is thought to tilt the moist inner core of the cyclone which produces downdrafts that advect aforementioned lower entropy environmental air into the boundary layer where that air is taken up by the cyclone's core [46], decreasing intensity by the mechanism explained above. Shear is estimated from 12 hourly ERA5 snapshots, and during integration the snapshot nearest in time is utilized. The velocity is averaged at the 250mbar and 850mbar pressure levels in a  $6^\circ$  radius about the center of the storm, following [7], and shear is computed as  $S = |\vec{u}_{250} - \vec{u}_{850}|$ . All other features are computed using monthly averaged ERA5 variables.

We use the FAST open source codebase [31] to compute these features and refer the reader to this source for further implementation details.

## 2.1 Equation Setup

Tropical cyclone intensity evolves dynamically as a function of the cyclone's internal state as well as the large-scale environment through which it moves. Following [31], we assume that a differential equation model of intensity  $v$

$$\dot{v} = F(v, \alpha, V_p, \chi, S) \quad (3)$$

can capture observed dynamics, where  $F$  is some function of the current intensity and aforementioned environmental variables. We nondimensionalize each variable by dividing by a characteristic scale

$$v' = \frac{v}{50 \text{ m s}^{-1}}, V_p' = \frac{V_p}{50 \text{ m s}^{-1}}, \chi' = \frac{\chi}{2 \text{ J K}^{-1} \text{ kg}^{-1}}, S' = \frac{S}{10 \text{ m s}^{-1}} \quad (4)$$

so that each variable is  $O(1)$ . We parameterize the function  $F$  as a polynomial of the input variables up to a particular degree. The functional relationship is

$$dv' = \underbrace{(\beta_0 + \beta_1 v' + \beta_2 v'^2 + \beta_3 v' V_p' + \beta_4 v' V_p'^2 + \cdots + \beta_{55} S'^3)}_{56 \text{ terms}} d\tau + \sigma'(v') dW_t \quad (5)$$

where each feature is a product of the nondimensionalized input variables and  $\tau = 6\text{h}$  is the observational timescale. The term  $\sigma'(v')$  is the standard deviation (of nondimensionalized intensity  $v'$ ) of a Wiener Process learned during a calibration step to model remaining uncertainties in intensification, and are detailed in Sec. 4.4.

In general, each feature is  $\phi_j = v'^{k_1} \alpha^{k_2} V_p'^{k_3} \chi'^{k_4} S'^{k_5}$  for integers  $\sum_j k_j \leq k_{max} = 3$ . All coefficients  $\beta_i$  have units  $\tau^{-1}$  by dimensional consistency. A range of polynomial degrees was attempted but validation error did not significantly decrease beyond degree 3.

Polynomial features are highly multicollinear so only a subset of terms may be necessary to capture the physical relationship. Hence, we seek a sparse solution, where a small subset of terms above have nonzero coefficients. Sparsity promotion is a means to regularize solutions and encourage generalization [27]. We detail the sparsity promotion procedure in Sec. 4.

$v' \alpha V'_p$	$\beta_0 = 1.53 \times 10^{-1} \tau^{-1}$
$v'$	$\beta_1 = -7.06 \times 10^{-2} \tau^{-1}$
$v' \alpha^2$	$\beta_2 = -6.70 \times 10^{-2} \tau^{-1}$
$v'^3$	$\beta_3 = -5.94 \times 10^{-2} \tau^{-1}$
$\alpha V'_p$	$\beta_4 = 5.02 \times 10^{-2} \tau^{-1}$
$\alpha V'^2_p$	$\beta_5 = -4.70 \times 10^{-2} \tau^{-1}$
$V'^3_p$	$\beta_6 = 1.26 \times 10^{-2} \tau^{-1}$
$V'^2_p S$	$\beta_7 = -1.16 \times 10^{-2} \tau^{-1}$
$\chi'^2$	$\beta_8 = -7.40 \times 10^{-3} \tau^{-1}$
$\chi'^3$	$\beta_9 = 1.20 \times 10^{-3} \tau^{-1}$

Table 1: Coefficient values of the sparse, learned equation.

### 3 Learned Intensification Model

Before we detail the methodology to learn the equation, we report it here. The model is

$$dv' = \underbrace{(\beta_0 v' \alpha V'_p + \beta_1 v' + \beta_2 v' \alpha^2 + \beta_3 v'^3 + \beta_4 \alpha V'_p + \beta_5 \alpha V'^2_p + \beta_6 V'^3_p + \beta_7 V'^2_p S' + \beta_8 \chi'^2 + \beta_9 \chi'^3)}_{10 \text{ terms}} d\tau + \sigma'(v') dW_t \quad (6)$$

and includes 10 terms from the original 56. As it is defined in the continuum, it can generate intensity values at arbitrary temporal resolution.

The deterministic component of the equation characterizes a stable fixed point in intensity. In the top panel of Fig. 1, we plot the ODE as a function of intensity  $v$  for a storm in conditions ripe for intensification, with high potential intensity  $V_p$ , high ocean heat content  $z$ , low environmental entropy deficit  $\chi$  and low vertical wind shear  $S$ . A single, stable fixed point is present at  $v = 64.5 \text{ m s}^{-1}$  which the cyclone will steadily approach.

The stable fixed point varies as a function of the environmental parameters and may be annihilated in conditions unfavorable to intensification. In the bottom of Fig. 1, we plot changes in the fixed point as a single environmental parameter is varied through a series of bifurcation plots. The stable fixed point increases with increased ocean heat content  $z$ , increasing potential intensity  $V_p$ , decreasing entropy deficit  $\chi$ , in agreement with expectations. Changes in wind shear  $S$  exhibit more interesting dynamics, as can be seen in the bottom right of Fig. 1. Above a threshold of wind shear  $S = 19 \text{ m s}^{-1}$  the lower unstable and upper stable fixed points annihilate in a saddle-node bifurcation and the storm gradually deintensifies at all intensities as long as the high wind shear persists. This behavior is consistent

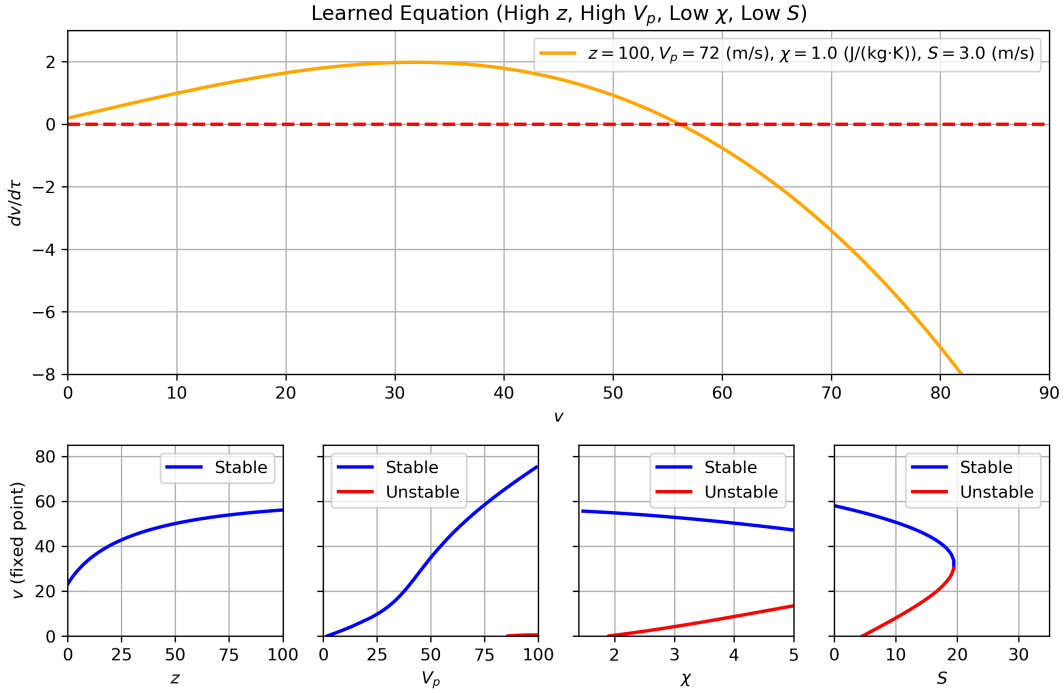


Figure 1: (Top) Plot of the learned differential equation as a function of intensity in conditions favorable to intensification, namely high upper ocean heat content  $z = 100.0$ , high potential intensity  $V_p = 72\text{ m s}^{-1}$ , low environmental entropy deficit  $\chi = 1.0\text{ J kg}^{-1}\text{ K}^{-1}$  and low wind shear  $S = 3.0\text{ ms}^{-1}$ . (Bottom) Bifurcation diagrams of the model as all parameters but one are varied. Parameter ranges are the complete range the parameters experience over all tracks.

with previous literature which found a  $20\text{m s}^{-1}$  threshold of vertical wind shear above which few storms intensify [51]. Dynamically, the saddle-node bifurcation is a novel elaboration on the bifurcation behavior of the FAST model [12], a physics-based TC intensification model. Prior work characterized all bifurcations in this model and did not identify a saddle-node bifurcation in wind shear [45]. FAST does not admit this behavior because in that model the time derivative of intensity  $\dot{v}$  decreases monotonically in  $v$  [12] for all parameter values so multiple fixed points are an impossibility. Future work can investigate the nonlinear dynamics of the learned model more closely.

### 3.1 Intensification Dynamics Comparison

Here we compare the intensification of historical storms to what the learned model predicts. We pick Hurricane Katrina (2008), Hurricane Luis (1995), and Typhoon Haiyan (2013) as test cases because each is a historically significant and damaging storm. The chosen storms are not in the training or validation sets. In Fig. 3.1 we plot the historical intensification and the probability contours of 100 synthetic storms generated along the same track using ERA5 reanalysis estimates of the surrounding environment. Each storm remains within the  $2\sigma$  contour over 93.75%, 97.8% and 100% of their duration, respectively.

Both Hurricane Katrina and Typhoon Haiyan underwent Rapid Intensification - a process where a storm increases in intensity by at least  $18\text{m s}^{-1}$  within a 24 hour period. The occurrence of Rapid Intensification empirically distinguishes the strongest storms from the weakest storms in terms of Lifetime Maximum Intensity (LMI) [30], hence its representation is key to capturing extreme events. While Rapid Intensification only occurs in large scale environmental conditions favorable to intensification [25], as measured by the environmental features used in our model, its timing is very challenging to predict [50] and, in high resolution numerical models, depends on state perturbations on the order of numerical modeling error [52]. Hence, while our model can capture the large scale climatological dependence of RI, it is not expected to precisely predict RI timing. That rapid intensification is included within the  $2\sigma$  ensemble suggests that the stochastic parameterization detailed in Sec. 4.4 can represent these challenging dynamics.

Next, we more systematically assess if simulated intensification matches the distribution of historical intensification. On a testing dataset of all Northern Hemisphere storms from 1979 to 2015, we simulate intensity along a historical IBTrACS track at each initial condition along the track and then scatter plot pairs of the synthetic and observed intensity in Fig. 3. If the statistics of simulated storms match that of observed storms, then the distribution

will be symmetric about the  $x = y$  line. We report the plot at time horizons of 6h, 24h and 72h and quantify the degree of symmetry by computing the Total Variation distance between a Gaussian KDE estimate of the distribution and its reflection. The Total Variation distance is

$$d_{tv}(P, Q) = \frac{1}{2} \sup_x |P(x) - Q(x)| \quad (7)$$

and measures the greatest discrepancy in probability afforded to the same event between two distributions. It is zero if the distributions match perfectly and 1 if they have disjoint supports. The total variation distance is  $d_{TV} = 0.0529, 0.0893, 0.2137$  for each time horizon, respectively. A persistence model at 6h, 24h and 66h time horizons achieve  $d_{TV} = 0.1912, 0.2469, 0.0813$ , respectively. This shows that the skill of persistence models is weak at sub 1 day time horizons, but that 3 day forecasts begin to decorrelate with initial intensities so their comparison approaches the distance between the marginal distribution of intensity with itself, which is  $d_{TV} = 0$ . At 6h and 24h, the distribution is strongly symmetrical, suggesting that the statistics of intensification match observations. At 72h, the bulk of the distribution is symmetrical except for a significant overestimation of Tropical Depressions (TDs,  $< 18 \text{ m s}^{-1}$ ). However, hurricane agencies often don't report Tropical Depressions or do so inconsistently [21], so our overestimation may reflect that if a storm becomes a Tropical Depression it is less likely to be reported in IBTrACS while our model's intensity is not lower bounded.

### 3.2 Climatological Comparison

Here, we assess aspects of Tropical Cyclone climatology and hazard as generated by the learned model. We generate 100 synthetic intensity time series per track over all IBTrACS tracks from 1979 to 2015. For the purposes of computing TC climatology, we treat this collection as 3600 years of storms (100 instances of the 36 year subset of IBTrACS). The intensity initial condition comes from the observed IBTrACS intensity, and environmental forcing comes from ERA5. In Fig. 4, we plot a single synthetic intensification series for each track in the testing dataset, restricted to times when the storm is a Tropical Storm or stronger ( $\geq 18 \text{ m s}^{-1}$ ). Visually, the most intense simulated storms are more intense than the most intense in IBTrACS, but the correspondence between storms at lower intensities is strong.

Next, we quantitatively assess climatological estimates of cyclone hazard. The Power Dissipation Index is a

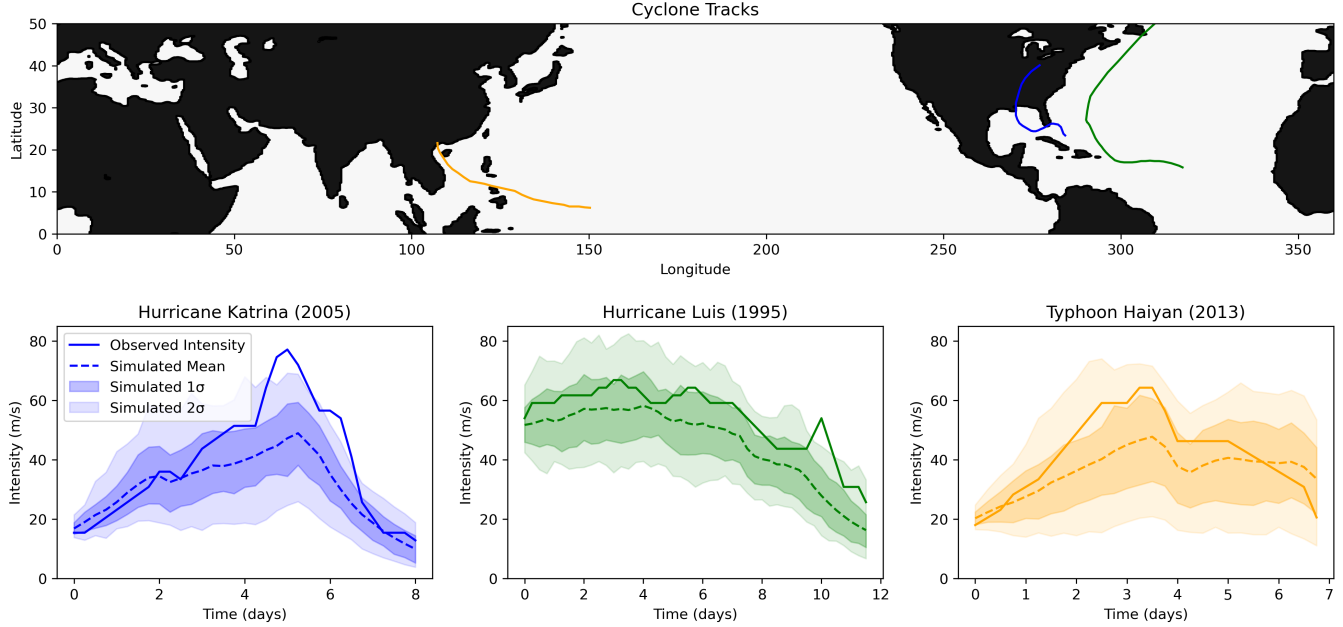


Figure 2: (Top) Three example Tropical Cyclone tracks from the IBTrACS dataset. (Bottom) IBTrACS intensities compared against the distribution of an ensemble of 100 synthetic storms for the same track and environmental forcings with confidence intervals.

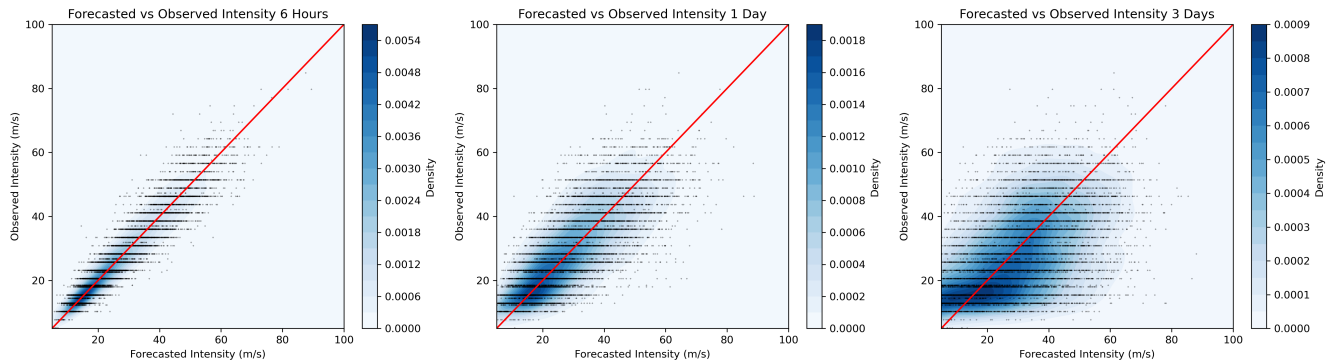


Figure 3: Scatter plot of forecasted versus observed IBTrACS intensities at time horizons of 6 hours, 1 day and 3 days on the testing dataset. A KDE estimate of the distribution is plotted in the background. IBTrACS is discretized to 5 knot increments.

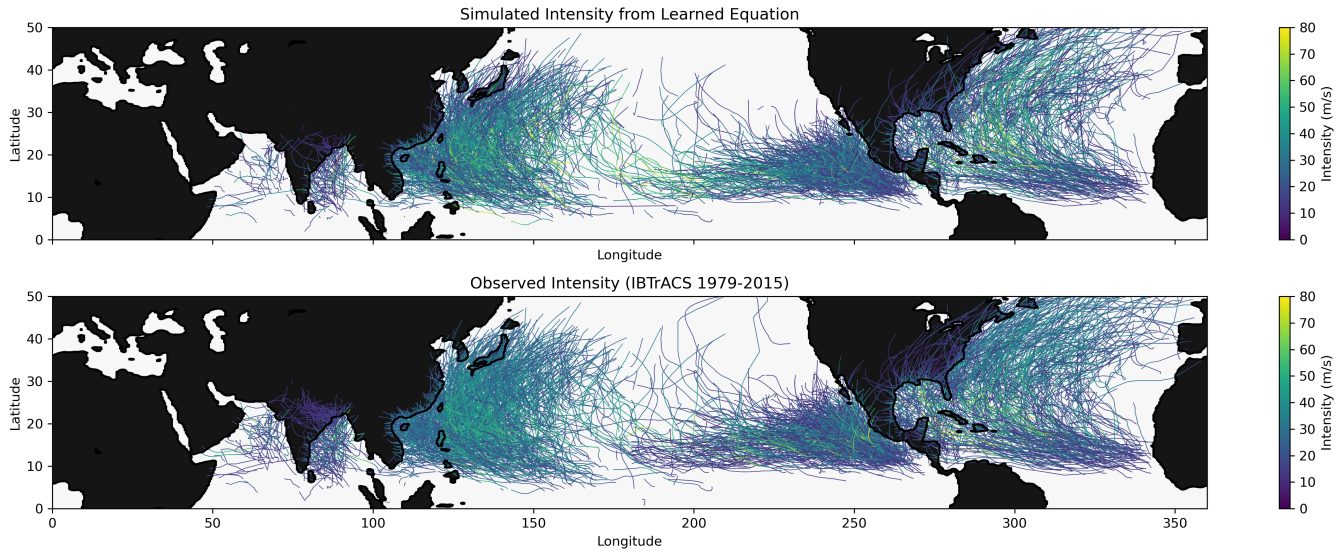


Figure 4: (Top) Synthetic intensification along a collection of testing IBTrACS tracks from 1982-2015. (Bottom) All tracks and intensities in the IBTrACS dataset, for comparison.

commonly used metric of hazard which is the integral of the cube of intensity over a cyclone’s lifetime

$$PDI = \int_0^\tau v(t)^3 dt.$$

The cube of intensity quantitatively captures that more extreme cyclones pose much greater hazard than smaller cyclones [14].

The Power Dissipation Index climatology for the Northern hemisphere using the learned model and observations is plotted in Figure 5. The PDI for a given year in a given basin is the sum of the integral above applied to every TC in a basin. To compute the figure, we treat each  $6^\circ \times 6^\circ$  degree region as a basin and take an annual average, using 1 simulated storm per IBTrACS track per year. The mean PDI over the domain for the learned climatology is 109.78% of the observational climatology, which confirms overestimation of intensity.

We also investigate the Lifetime Maximum Intensity Distribution for IBTrACS and the learned model in Fig. 7. Agreement is strong for all storms at or below  $65\text{m s}^{-1}$ , but there is overestimation of extreme LMIs. This can be attributed to the standard deviation of stochastic perturbations increasing linearly with intensity as determined in Sec. 4.4, which likely makes perturbations too extreme at extreme intensities and artificially inflates LMI.

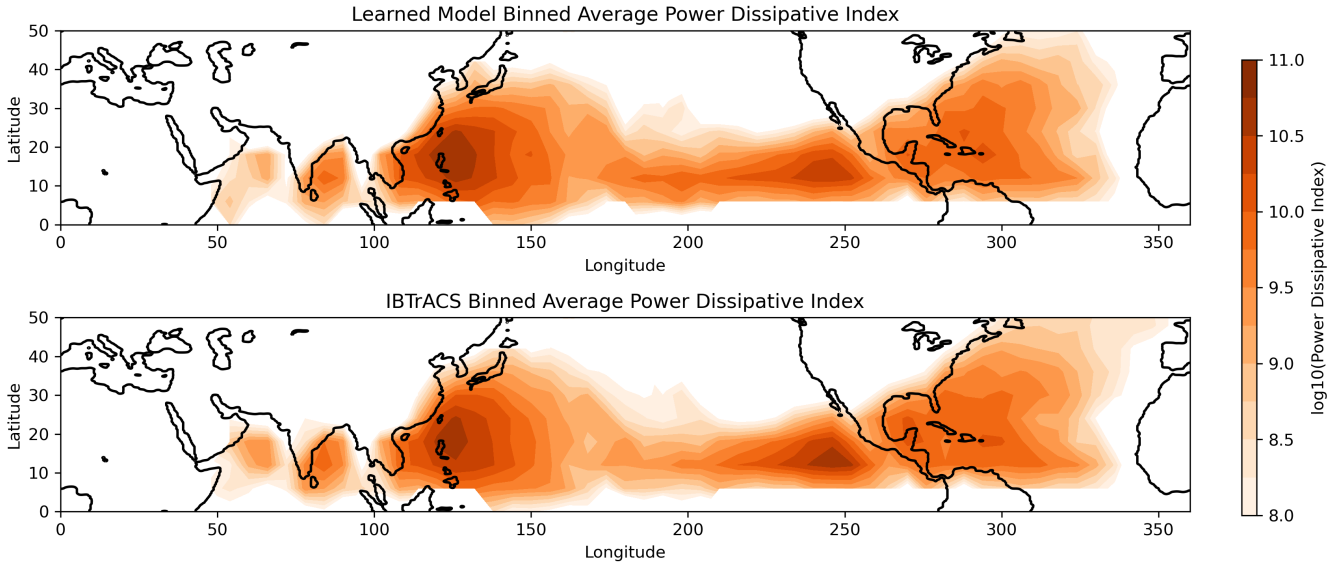


Figure 5: Power Dissipation Index climatology for learned model (top) and IBTrACS (bottom). PDI is computed in  $6^\circ \times 6^\circ$  boxes the contour plotted. Each PDI plot is an average of 3600 and 38 years respectively.

### 3.3 Landfalling Statistics

Next, we test the statistics of intensity at landfall. In Fig. 8, we estimate a continuous density of intensity at landfall for a collection of populous coastal cities, measured as all intensity values of storms within 150km of the city. Next, we estimate a histogram of landfalling intensities based on the whole IBTrACS dataset, using the 5 knot discretization of IBTrACS to set bin sizes. Then, we compute the KL-Divergence of the synthetic KDE against the IBTrACS histogram

$$D_{KL}(p_{obs} || q_{synth}) = \sum_i p_{obs}(v_i) \log_2 \left( \frac{p_{obs}(v_i)}{q_{synth}(v_i)} \right) \quad (8)$$

where  $p_{obs}$  is the histogram of IBTrACS intensities at landfall and  $q_{synth}$  is the modelled density. We report the divergence in bits as well as the entropy  $H = \sum_i p_i \log_2(1/p_i)$  of the IBTrACS histogram for comparison. We find that the match is strong for all cities except for Tokyo, where intensity is clearly underestimated, and Dhaka, where the most extreme storm observed is afforded low probability.

### 3.4 Return Period Assessment

We compute return period curves for a collection of important cities in Fig. 6. We utilize the Weibull formula [33] which calculates the annual exceedance probability as

$$P(v_i) = \frac{i}{n+1} \frac{n}{m} \quad (9)$$

where  $v_i$  is the  $i$ th highest intensity in a region over the simulated climatology duration,  $n$  is the total number of storms in that region, and  $m$  is the duration of the climatology in years. The return period is then the reciprocal of the exceedance probability. Return periods are computed over the IBTrACS dataset from 1979 to 2015 and over the testing dataset with 100 synthetic tracks per real track, which we treat as 3600 years of synthetic storms. The maximum intensity of storms while they are within 150km of the city of interest is retained.

There is agreement between observed and synthetic return periods for Shanghai, Kingston, Miami, Boston, Dhaka and Chittagong, but disagreement in Tokyo, Hong Kong, Manila and Taipei. In Tokyo, the return period of storms under  $35\text{ m s}^{-1}$  is overestimated. In Hong Kong, Manila and Taipei - all Tropical cities in the North Western Pacific basin - return periods of storms above  $45\text{ m s}^{-1}$  are significantly overestimated compared to observations, suggesting a positive bias in the most extreme storm events in this basin, which can again be attributed to our stochastic parameterization from Sec. 4.4 as with the LMI distribution. Meanwhile, the return period of storms approaching Tokyo is overestimated, perhaps due to the inclusion of a damping term  $V_p S$  which scales damping due to wind shear by the potential intensity which is highest in the Western Pacific basin.

## 4 Equation Learning

Equation learning proceeds in 3 steps. First, we select features by solving an Integral SINDy problem [5, 44]. Second, we refit the parameters of the chosen features using an Ensemble Kalman Filter as a fine-tuning step [48]. Third, we calibrate a stochastic component to represent unresolved intensification processes.

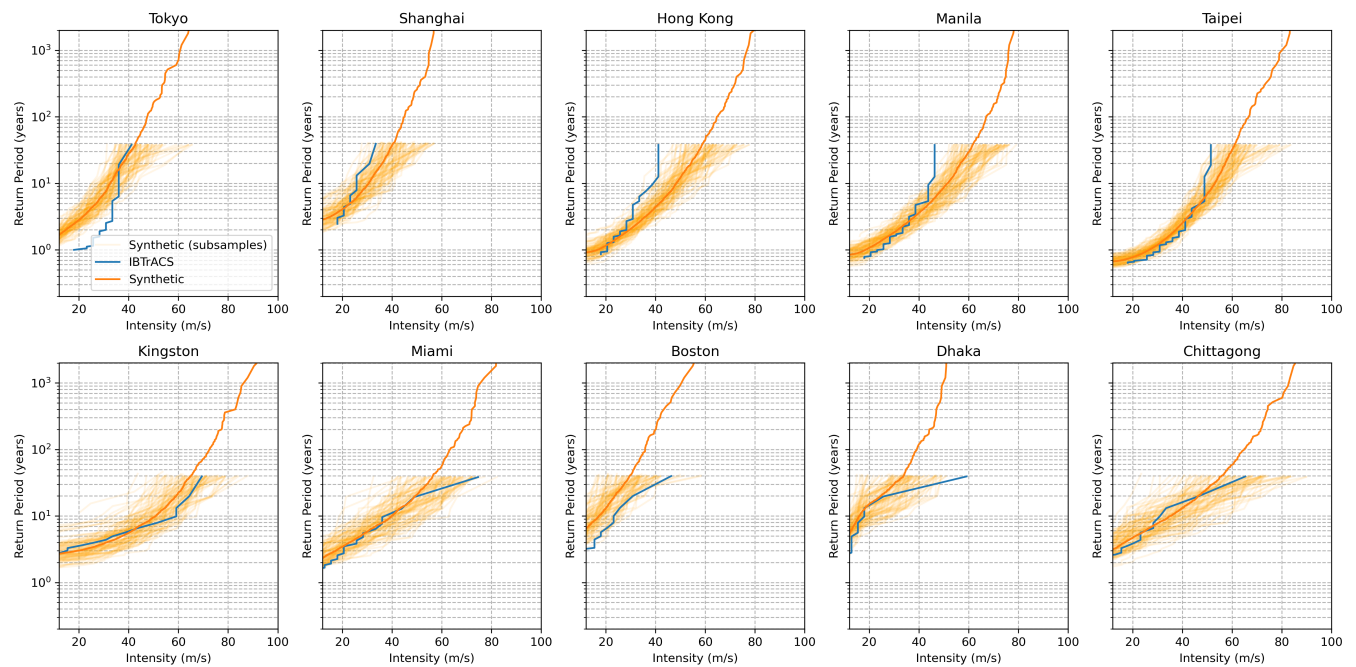


Figure 6: Return period curves for a radius of 150km region around a large collection of populous cities in the Northern Hemisphere.

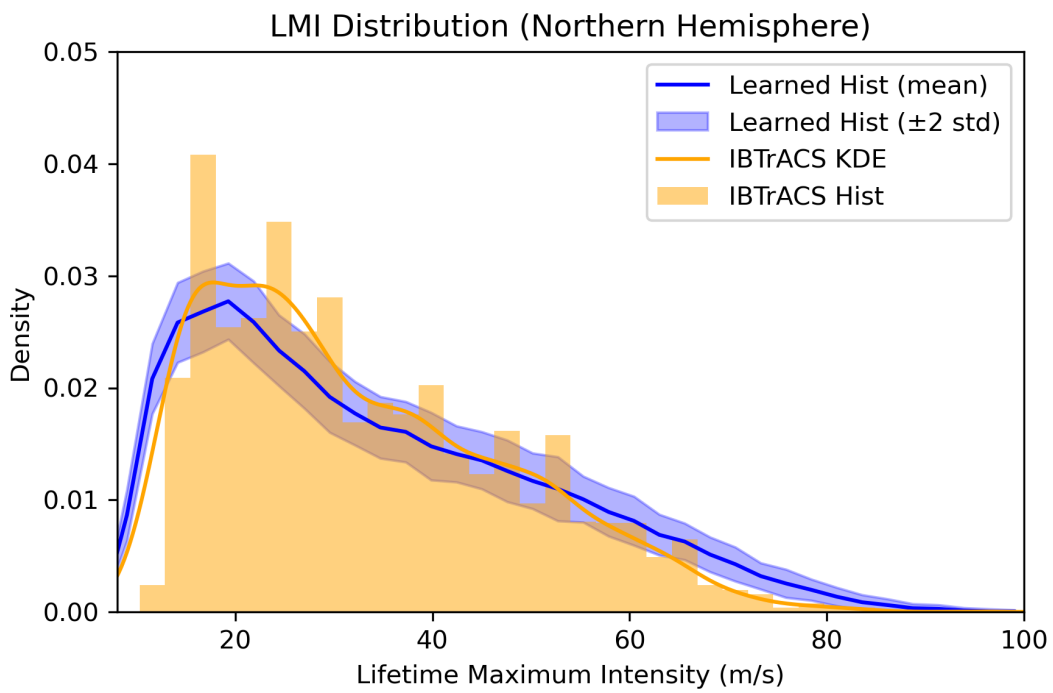


Figure 7: The Lifetime Maximum Intensity distribution of the IBTrACS dataset in the Northern Hemisphere, from 1979-2015. Corresponding distribution for synthetic climatology generated from the learned model with uncertainty found by subsampling the learned model to the size of the IBTrACS dataset.

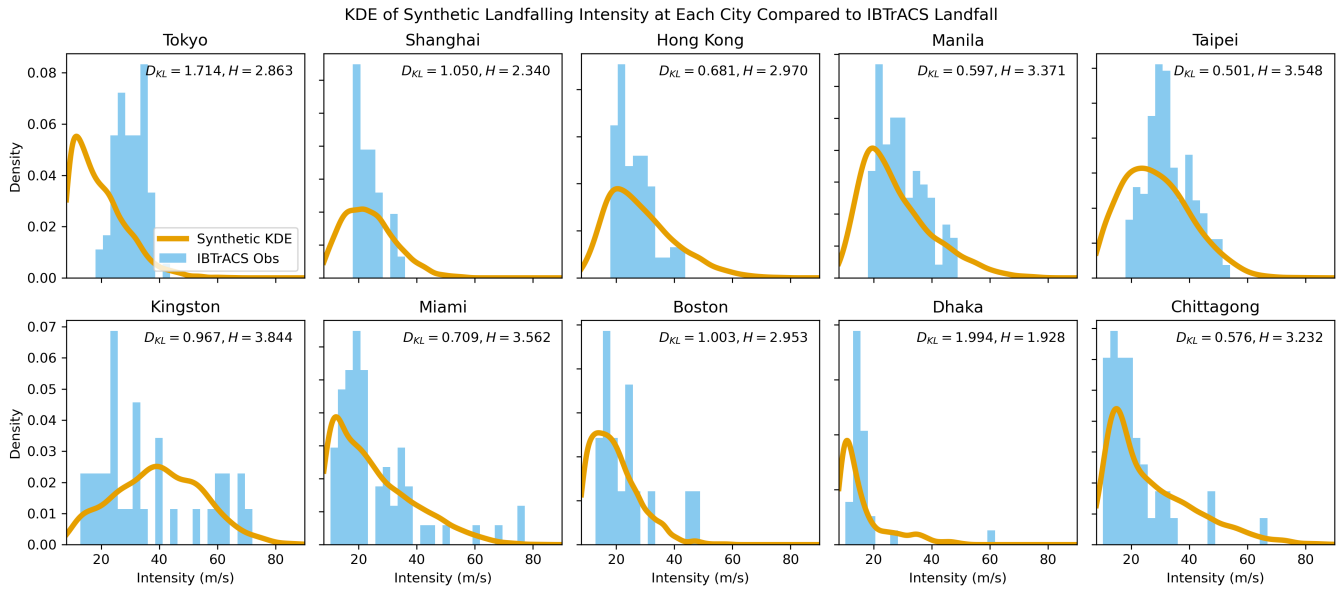


Figure 8: Intensity distribution of storms a 150km radius of a collection of major cities for IBTrACS historical data and from the collection of synthetic storms. The KL Divergence from the historical to synthetic KDE is reported in each case.

#### 4.1 Integral SINDy

We use Integral SINDy [44] to identify the subset of terms for use in the intensification model. Integral SINDy sets up a sparse linear regression problem by using the integral formulation of an inhomogeneous differential equation  $\dot{x} = F(x, t)$  which is

$$x(t_i + T) - x(t_i) = \int_0^T F(x(t' + t_i), t' + t_i) dt' \quad (10)$$

for a time horizon  $T$  and for any initial time  $t_i$ . Assuming the linear model structure for  $F(x(\tau), \tau)$  from Eq. 5, we have that  $F(x(t), t) = \sum_j \beta_j \phi_j(x(t), t)$  for features  $\phi_j$  which lets us move the integral in Eq. 10 over all individual features

$$x(t_i + T) - x(t_i) = \sum_j \beta_j \int_0^T \phi_j(x(t' + t_i), t' + t_i) dt'. \quad (11)$$

If we denote each integral term as  $d_{j,i,T} = \int_0^T \phi_j(x(t' + t_i), t' + t_i) dt'$  and each time difference as  $C_{i,T} = x(t_i +$

$T) - x(t_i)$ , we find a set of linear equations

$$C_{i,T} = \sum_j \beta_j d_{j,i,T}. \quad (12)$$

We estimate the temporal differences in intensity  $C_{i,T}$  directly from IBTrACS intensity time series. Each integral is approximated using piecewise constant quadrature over the 6 hour time increments in the data  $\int_0^T \phi_j(x(t'+t_i), t'+t_i) dt' \approx \sum_{k=0}^{T/\Delta t} \phi_j(x(k\Delta t+t_i), k\Delta t+t_i) \Delta t$  for  $\Delta t = 6h$ . Piecewise constant quadrature is used because it averages out observation noise in the integrated terms [44]. We use the intensity from IBTrACS and the environmental variables from ERA5 dataset to compute  $\phi_j(x(k\Delta t+t_i), k\Delta t+t_i)$ .

Note that a linear equation can be produced for every initial condition and for every valid time horizon  $T$  from that initial condition. This means we can produce an abundance of constraints - by using all storms from 2016 to 2020 and with a maximum time horizon of  $T = 5$  days, we create  $n = 71,553$  rows. We seek a sparse solution which minimizes

$$\hat{\beta} = \arg \min_{\beta} \|C - \beta D\| \quad s.t. \quad \ell_0(\beta) \leq k \quad (13)$$

for some subset size  $k$  and  $C, D$  are flattened matrix representations of Eq. 12.

This is a Best Subset Selection problem [53]. In general, this problem is NP-Hard [9] due to concavity of the regularization penalty. A variety of greedy approximate algorithms are available such as Matching Pursuit [34], Orthogonal Matching Pursuit [6], and Least-Absolute Shrinkage and Selection Operator (LASSO) [20]. Advances in Mixed Integer Quadratic Programming solvers has enabled tractable global solutions for some problems [2]. We use the recently developed Absolute Best-Subset Selection (ABESS) algorithm because of its computational efficiency and favorable convergence properties [53].

To assess how many terms to include, we plot the cost using 5-fold cross validation over the training dataset as a function of the number of included terms  $k$  in Figure 10. We select  $k = 10$  terms as a tradeoff between skill and model complexity and find a 38% reduction in error compared to persistence on the validation dataset. The model is trained using IBTrACS storms from 2016 to 2020 which have been matched to ERA5 counterparts [21]. The training-validation split is 90% – 10% and storms are chosen at random. The testing dataset is all storms from 1979 to 2015.

## 4.2 Parameter Fine-Tuning

We fine-tune the parameters for the chosen 10 terms using an Ensemble Kalman Update. In the terminology of [48], this step realizes the ensemble-based inference component of the informative learning cycle, using the ensemble Kalman update as an adjoint-free parameter estimator for the nonlinear TC intensification model.

The Ensemble Kalman Update is a generalization of the Kalman Update which assumes that an observation is a linear function of the latent parameter of interest, contaminated by observation noise [23]

$$y = H\beta + \nu \quad (14)$$

where  $H$  is a linear map and  $\nu \sim \mathcal{N}(0, C_{\nu\nu})$  is Gaussian observation noise assumed independent from the underlying parameters  $\beta$ . The Ensemble Kalman Update extends the linear Kalman update by using an ensemble to make a linear approximation  $H$  of a nonlinear observation mapping  $h$ .

Let the ensemble of 10 parameters  $\beta$  be samples from a Gaussian prior  $\beta \sim \mathcal{N}(\beta^-, C_{\beta\beta}^-)$  and denote the ensemble itself as  $X = [\beta_1 \ \beta_2 \ \dots \ \beta_E]$  where  $E$  is our ensemble size. By integrating the intensification model defined by each  $\beta_i$  from an initial condition at time  $t_i$  to a later point in time  $t_i + T$ , which we represent by the nonlinear function  $h(\cdot)$ , we can compute an ensemble of predicted intensities  $Y = [h(\beta_1) \ h(\beta_2) \ \dots \ h(\beta_E)]$  for an observed intensity  $y = v_{\text{IBTrACS}}(t_i + T)$ .

Given a prior ensemble over coefficients  $\beta^-$  of dimension  $10 \times E$ , the Ensemble Kalman update is

$$\beta^+ = \beta^- + K'(y - Y) \quad (15)$$

where the Kalman Gain matrix  $K$  [42] is computed using the ensemble as

$$K' = \frac{1}{N-1} \tilde{\beta} \tilde{Y}^T \left( \frac{1}{N-1} \tilde{Y} \tilde{Y}^T + C_{\nu\nu} \right). \quad (16)$$

We chose observation noise covariance as  $C_{\nu\nu} = I\sigma^2$  where  $\sigma = 2.57\text{m/s}$  to reflect the discretization of intensity in IBTrACS, which is binned to 2.57m/s increments. In general, this linear approximation in the Ensemble Kalman Update is not guaranteed to converge for nonlinear systems [8]. As our observation function involves the integration

of a nonlinear dynamical system, our procedure is therefore not guaranteed to converge, however, empirically the ensemble Kalman Update has been successfully used for data assimilation in many nonlinear systems in geosciences [24]. After parameter fine-tuning, the model achieves a 37.6% improvement in 3 day ahead intensity forecasts on the validation dataset compared to a persistence model.

### 4.3 Model Training

Our training data consists of 5 years of ERA5 data from 2016 to 2020 restricted to TCs in the Northern Hemisphere. To simulate a cyclone, the intensification ODE is forced by time-dependent environmental variables from ERA5 along the track of an IBTrACS cyclone. At a particular training step, the model’s intensity is initialized to the IBTrACS intensity at a point along an observed track and the whole ensemble  $[\vec{\beta}_1, \vec{\beta}_2, \dots, \vec{\beta}_E]$  is integrated 6 hours into the future. The ensemble size is  $E = 100$ . The Kalman Learner update is batched over 16 initial conditions to mitigate the EnKF’s tendency to be overconfident [42]. We then perform 11 more epochs of training, each at a time horizon from 12 hours to 3 days in 6 hour increments. Such rollout is crucial for model stability. We retain only the mean of the resulting posterior of coefficients as the final parameter values, so system stochasticity arises only from the model’s stochastic component, which is learned in Sec. 4.4. With CPU-only parallelization over ensemble members, this training step takes 17h.

### 4.4 Calibration

Here we parameterize the unresolved components of Tropical Cyclone intensification in a calibration step. We first compute the residuals of the trained deterministic model on one day ahead forecasts on the validation dataset. A plot of the residuals is included in Fig. 9. By first binning the residuals into 6 bins with equal numbers of samples, we observe a linear relationship between the intensity and the standard deviation of the residuals. Significant bias is present only at intensities below  $14\text{m s}^{-1}$ , in the range of TDs, but we do not believe this bias is genuine due to the TD reporting concerns mentioned in Sec. 3.1. Hence, we do not bias correct the model. Using linear regression, we find an expression for the standard deviation of intensity, which is  $\sigma(v) = 0.110v + 0.229\text{m s}^{-1}$ . We then nondimensionalize to  $\sigma'(v') = \sigma(v)/50\text{m s}^{-1} = 0.110v' + 4.58 \times 10^{-3}$  and add the stochastic component  $\sigma'(v')dW_t$  to the model.

While the empirical calibration captures stochasticity at intensities below  $42\text{m s}^{-1}$  (the lower boundary of the most intense bin), we do not have enough data to assess how well it extrapolates to more extreme intensities. This

choice likely contributes to overestimation of LMI (Fig. 7) and overestimation of extreme storm return periods (Fig. 6) in the Western Pacific.

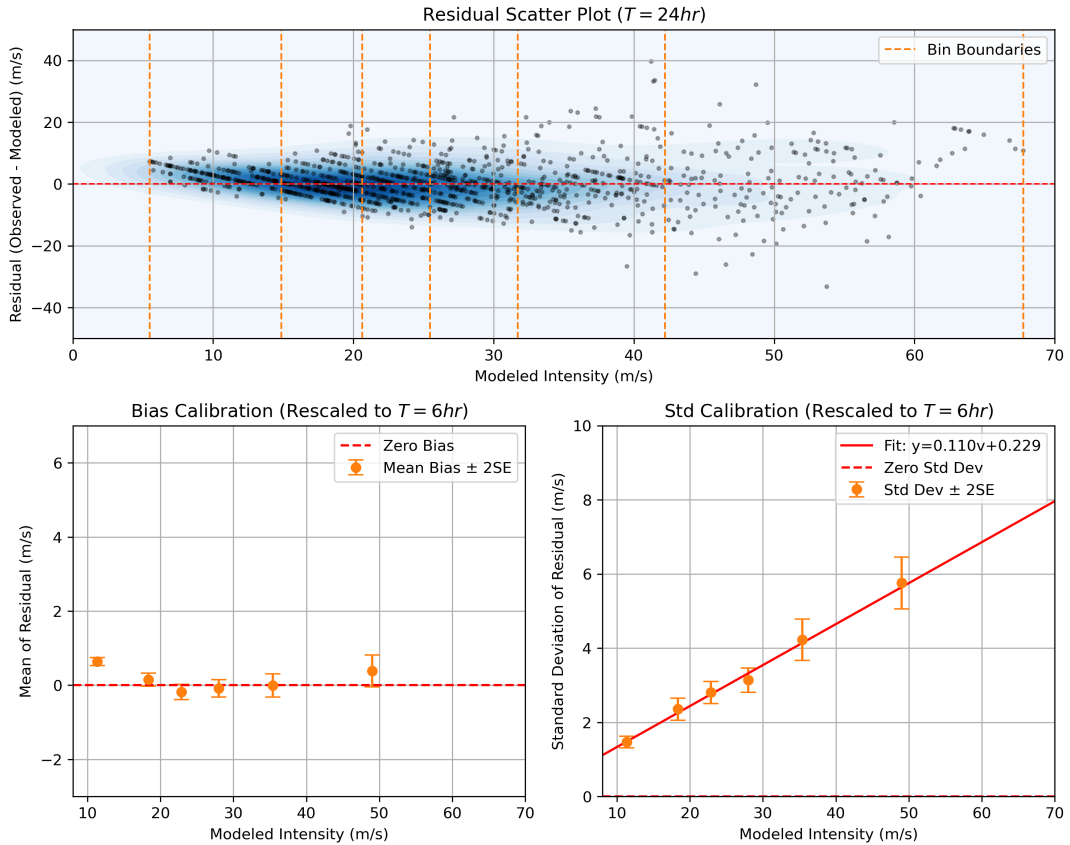


Figure 9: (Top) Distribution of residuals over a single 6h time step computed over the validation dataset. Bin boundaries are specified as orange vertical lines. (Bottom Left) The mean residual in each bin, and bootstrapped standard errors using 1000 resamplings. (Bottom Right) The residual standard deviation also with bootstrapped standard errors using 1000 resamplings. Linear fit was found using weight linear regression with weights set by the standard error bars.

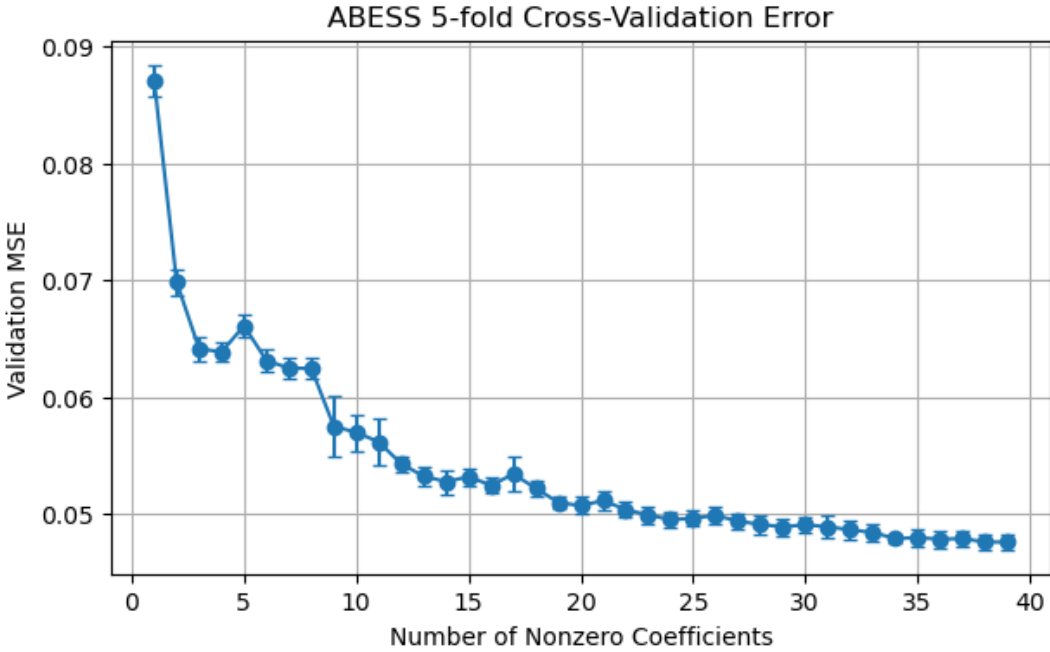


Figure 10: Validation error of sparse solutions as a function of the number of included terms. Used 5-fold cross validation on the training dataset.

## 5 Discussion and Future Directions

In this paper, we showed that

1. A nonlinear system identification pipeline can identify a predictive and interpretable physics-style differential equation model of TC intensification from simulations and observations.
2. The model generates a synthetic climatology that captures many aspects of observed TC climatology.
3. The learned equation suggests a novel saddle-node bifurcation of intensity in wind shear which is not present in existing physical models.

The model produces non-divergent synthetic intensity tracks which can be used to generate a Tropical Cyclone climatology (Fig. 4). Over historical tracks, the synthetic climatology matches observations for much of the Lifetime Maximum Intensity distribution (Fig. 7), return period curves for many cities (Fig. 6) and intensities of storms

at landfall (Fig. 8). The model exhibits notable biases, such as overestimation of return periods for weak storms about Tokyo, underestimation of return periods of the strongest storms in the North Western Pacific basin, and overestimation of lifetime maximum intensities above  $65\text{m s}^{-1}$ . These biases likely come from our strong structural assumptions, such as a sparse polynomial deterministic component (Sec. 3) and linearity in the stochastic noise standard deviation (Sec. 4.4). Though this is a machine learning model, we intentionally imposed a restricted model structure for the sake of interpretability which could be sacrificed with a more flexible structure, such as a Neural Network, to further alleviate bias. Further, greater access to information (whether from more historical data, CAM simulations or theory) is needed to verify the stochasticity parameterization at extreme intensity values. That said, our stochastic parameterization does capture the process of rapid intensification, which is a key process for representing the most extreme storms [30]. Rapid intensification cannot be predicted precisely from our set of coarse-grained environmental variables [36], however, prior work which forecasts Rapid Intensification using memory of past TC states has shown enhanced skill [50], which indicates RI could be better predicted with the inclusion of latent variable tracking the state of the storm’s core. Adding a learned latent variable to our intensity model, such as inner core moisture as in the FAST model [12], could enhance the representation of RI and model skill more generally.

The model, being a polynomial SDE, it is ripe for mathematical analysis. In particular, a nonlinear dynamics bifurcation analysis, which we begin in this paper in Fig. 1, can characterize tipping points or other nontrivial nonlinear dynamics in the model. We identified a Saddle Node bifurcation as wind shear  $S$  increases where the stable fixed point in intensity vanishes. This behavior is consistent with observations [51] and is a novel elaboration on the dynamics in the FAST model [12, 45], a leading physics-based model. Our result shows that system-identification techniques can uncover interesting dynamics in complex natural systems and motivate future work to investigate the physics of this empirical finding.

The model has potential to be used in hazard estimation pipelines. The model can be run very quickly as it is a concise SDE and, in principle, the model could be forced by monthly-mean or scenario-based climatological fields, making it lightweight for hazard projections once suitable environmental estimates are available. Separate genesis and track generation components will need to be specified to complete this pipeline, which can also be learned with system identification approaches in future work. However, tests of its generalizability (say under climate-change change forcings or in Southern Hemisphere basins) and closer scrutiny of its regional biases are needed before it can

be safely used in a hazard pipeline.

Though a performant model has been learned, it depends on pre-engineered features which greatly simplified the model learning process. Application of system identification techniques to less well understood problems, such as Extratropical Cyclone intensification, will require an additional feature learning step from primitive climate model outputs. Such a pipeline has the potential to identify novel physical features which govern intensification and present them in an interpretable low-order model which could enhance predictive skill and physical understanding.

We hope that this work opens the door to using nonlinear system identification techniques to identify data and theory driven models of Earth System dynamics. Such models may find otherwise opaque predictive regularities, represent them in a transparent form, and hence accelerate physical model development.

## References

- [1] Mario C. Acosta et al. “The computational and energy cost of simulation and storage for climate science: lessons from CMIP6”. English. In: *Geoscientific Model Development* 17.8 (Apr. 2024). Publisher: Copernicus GmbH, pp. 3081–3098. ISSN: 1991-959X. DOI: 10.5194/gmd-17-3081-2024. URL: <https://gmd.copernicus.org/articles/17/3081/2024/> (visited on 12/18/2025).
- [2] Dimitris Bertsimas and Wes Gurnee. “Learning sparse nonlinear dynamics via mixed-integer optimization”. en. In: *Nonlinear Dynamics* 111.7 (Apr. 2023), pp. 6585–6604. ISSN: 1573-269X. DOI: 10.1007/s11071-022-08178-9. URL: <https://doi.org/10.1007/s11071-022-08178-9> (visited on 01/16/2025).
- [3] M. Bister and K. A. Emanuel. “Dissipative heating and hurricane intensity”. en. In: *Meteorology and Atmospheric Physics* 65.3 (Sept. 1998), pp. 233–240. ISSN: 1436-5065. DOI: 10.1007/BF01030791. URL: <https://doi.org/10.1007/BF01030791> (visited on 04/11/2025).
- [4] Nadia Bloemendaal et al. “Generation of a global synthetic tropical cyclone hazard dataset using STORM”. en. In: *Scientific Data* 7.1 (Feb. 2020). Publisher: Nature Publishing Group, p. 40. ISSN: 2052-4463. DOI: 10.1038/s41597-020-0381-2. URL: <https://www.nature.com/articles/s41597-020-0381-2> (visited on 05/27/2025).
- [5] Steven L. Brunton, Joshua L. Proctor, and J. Nathan Kutz. “Discovering governing equations from data by sparse identification of nonlinear dynamical systems”. In: *Proceedings of the National Academy of Sciences* 113.15 (Apr. 2016). Publisher: Proceedings of the National Academy of Sciences, pp. 3932–3937. DOI: 10.1073/pnas.1517384113. URL: <https://www.pnas.org/doi/10.1073/pnas.1517384113> (visited on 09/02/2025).
- [6] T. Tony Cai and Lie Wang. “Orthogonal Matching Pursuit for Sparse Signal Recovery With Noise”. en. In: *IEEE Transactions on Information Theory* 57.7 (July 2011), pp. 4680–4688. ISSN: 0018-9448, 1557-9654. DOI: 10.1109/TIT.2011.2146090. URL: <http://ieeexplore.ieee.org/document/5895106/> (visited on 08/26/2025).

[7] Shuyi S. Chen, John A. Knaff, and Frank D. Marks. “Effects of Vertical Wind Shear and Storm Motion on Tropical Cyclone Rainfall Asymmetries Deduced from TRMM”. EN. In: *Monthly Weather Review* 134.11 (Nov. 2006). Publisher: American Meteorological Society Section: Monthly Weather Review, pp. 3190–3208. ISSN: 1520-0493, 0027-0644. DOI: 10.1175/MWR3245.1. URL: <https://journals.ametsoc.org/view/journals/mwre/134/11/mwr3245.1.xml> (visited on 11/21/2025).

[8] Dan Crisan and Boris L’vovich Rozovskii. *The Oxford handbook of nonlinear filtering*. eng. OUP Catalogue. Oxford ; New York: Oxford University Press, 2011. ISBN: 978-0-19-953290-2.

[9] G. Davis, S. Mallat, and M. Avellaneda. “Adaptive greedy approximations”. en. In: *Constructive Approximation* 13.1 (Mar. 1997), pp. 57–98. ISSN: 1432-0940. DOI: 10.1007/BF02678430. URL: <https://doi.org/10.1007/BF02678430> (visited on 08/26/2025).

[10] Mark DeMaria and John Kaplan. “A Statistical Hurricane Intensity Prediction Scheme (SHIPS) for the Atlantic Basin”. EN. In: *Weather and Forecasting* 9.2 (June 1994). Publisher: American Meteorological Society Section: Weather and Forecasting, pp. 209–220. ISSN: 1520-0434, 0882-8156. DOI: 10.1175/1520-0434(1994)009<0209:ASHIPS>2.0.CO;2. URL: [https://journals.ametsoc.org/view/journals/wefo/9/2/1520-0434\\_1994\\_009\\_0209\\_aships\\_2\\_0\\_co\\_2.xml](https://journals.ametsoc.org/view/journals/wefo/9/2/1520-0434_1994_009_0209_aships_2_0_co_2.xml) (visited on 12/19/2025).

[11] ECMWF. *IFS Documentation CY49R1 - Part I: Observations*. en. text. 2024. URL: <https://www.ecmwf.int/en/elibrary/81623-ifs-documentation-cy49r1-part-i-observations> (visited on 12/18/2025).

[12] Kerry Emanuel. “A fast intensity simulator for tropical cyclone risk analysis”. en. In: *Natural Hazards* 88.2 (Sept. 2017), pp. 779–796. ISSN: 1573-0840. DOI: 10.1007/s11069-017-2890-7. URL: <https://doi.org/10.1007/s11069-017-2890-7> (visited on 10/08/2024).

[13] Kerry Emanuel. “Climate and Tropical Cyclone Activity: A New Model Downscaling Approach”. en. In: (Oct. 2006). Section: *Journal of Climate*. DOI: 10.1175/JCLI3908.1. URL: <https://journals.ametsoc.org/view/journals/clim/19/19/jcli3908.1.xml> (visited on 06/19/2025).

[14] Kerry Emanuel. “Increasing destructiveness of tropical cyclones over the past 30 years”. en. In: *Nature* 436.7051 (Aug. 2005). Publisher: Nature Publishing Group, pp. 686–688. ISSN: 1476-4687. DOI: 10.1038/nature03906. URL: <https://www.nature.com/articles/nature03906> (visited on 05/10/2025).

[15] Kerry Emanuel. “Tropical Cyclones”. en. In: *Annual Review of Earth and Planetary Sciences* 31.1 (May 2003), pp. 75–104. ISSN: 0084-6597, 1545-4495. DOI: 10.1146/annurev.earth.31.100901.141259. URL: <https://www.annualreviews.org/doi/10.1146/annurev.earth.31.100901.141259> (visited on 01/28/2025).

[16] Kerry Emanuel and Fuqing Zhang. “On the Predictability and Error Sources of Tropical Cyclone Intensity Forecasts”. EN. In: *Journal of the Atmospheric Sciences* 73.9 (Sept. 2016). Publisher: American Meteorological Society Section: *Journal of the Atmospheric Sciences*, pp. 3739–3747. ISSN: 0022-4928, 1520-0469. DOI: 10.1175/JAS-D-16-0100.1. URL: <https://journals.ametsoc.org/view/journals/atsc/73/9/jas-d-16-0100.1.xml> (visited on 12/18/2025).

[17] Kerry Emanuel et al. “Environmental Control of Tropical Cyclone Intensity”. en. In: (Apr. 2004). Section: *Journal of the Atmospheric Sciences*. ISSN: 1520-0469. URL: [https://journals.ametsoc.org/view/journals/atsc/61/7/1520-0469\\_2004\\_061\\_0843\\_ecotci\\_2.0.co\\_2.xml](https://journals.ametsoc.org/view/journals/atsc/61/7/1520-0469_2004_061_0843_ecotci_2.0.co_2.xml) (visited on 08/08/2025).

[18] Kerry A. Emanuel. “Thermodynamic control of hurricane intensity”. en. In: *Nature* 401.6754 (Oct. 1999). Publisher: Nature Publishing Group, pp. 665–669. ISSN: 1476-4687. DOI: 10.1038/44326. URL: <https://www.nature.com/articles/44326> (visited on 05/28/2024).

[19] ERA5 hourly data on single levels from 1940 to present. en. URL: <https://cds.climate.copernicus.eu/datasets/reanalysis-era5-single-levels?tab=overview> (visited on 12/12/2025).

[20] Trevor Hastie, Robert Tibshirani, and Martin Wainwright. *Statistical Learning with Sparsity: The Lasso and Generalizations*. New York: Chapman and Hall/CRC, May 2015. ISBN: 978-0-429-17158-1. DOI: 10.1201/b18401.

[21] Kevin Hodges, Alison Cobb, and Pier Luigi Vidale. “How Well Are Tropical Cyclones Represented in Reanalysis Datasets?” EN. In: *Journal of Climate* 30.14 (July 2017). Publisher: American Meteorological Society Section: Journal of Climate, pp. 5243–5264. ISSN: 0894-8755, 1520-0442. DOI: 10.1175/JCLI-D-16-0557.1. URL: <https://journals.ametsoc.org/view/journals/clim/30/14/jcli-d-16-0557.1.xml> (visited on 03/11/2024).

[22] “Identification of Coupled Map Lattice and Partial Differential Equations of Spatio-temporal Systems”. en. In: *Nonlinear System Identification*. Section: 13\_eprint: <https://onlinelibrary.wiley.com/doi/pdf/10.1002/978118535561.ch13>. John Wiley & Sons, Ltd, 2013, pp. 431–472. ISBN: 978-1-18-53556-1. DOI: 10.1002/978118535561.ch13. URL: <https://onlinelibrary.wiley.com/doi/abs/10.1002/978118535561.ch13> (visited on 10/16/2025).

[23] R. E. Kalman. “A New Approach to Linear Filtering and Prediction Problems”. In: *Journal of Basic Engineering* 82.1 (Mar. 1960), pp. 35–45. ISSN: 0021-9223. DOI: 10.1115/1.3662552. URL: <https://doi.org/10.1115/1.3662552> (visited on 09/11/2025).

[24] Eugenia Kalnay. *Atmospheric Modeling, Data Assimilation and Predictability*. Publication Title: Atmospheric Modeling ADS Bibcode: 2002amda.book.....K. Dec. 2002. URL: <https://ui.adsabs.harvard.edu/abs/2002amda.book.....K> (visited on 01/13/2026).

[25] John Kaplan et al. “Evaluating Environmental Impacts on Tropical Cyclone Rapid Intensification Predictability Utilizing Statistical Models”. en. In: (Oct. 2015). Section: Weather and Forecasting. DOI: 10.1175/WAF-D-15-0032.1. URL: [https://journals.ametsoc.org/view/journals/wefo/30/5/waf-d-15-0032\\_1.xml](https://journals.ametsoc.org/view/journals/wefo/30/5/waf-d-15-0032_1.xml) (visited on 10/23/2024).

[26] Kenneth R. Knapp et al. “The International Best Track Archive for Climate Stewardship (IBTrACS)”. en. In: (Mar. 2010). Section: Bulletin of the American Meteorological Society. DOI: 10.1175/2009BAMS2755.1. URL: [https://journals.ametsoc.org/view/journals/bams/91/3/2009bams2755\\_1.xml](https://journals.ametsoc.org/view/journals/bams/91/3/2009bams2755_1.xml) (visited on 09/10/2025).

[27] J. Nathan Kutz and Steven L. Brunton. “Parsimony as the ultimate regularizer for physics-informed machine learning”. en. In: *Nonlinear Dynamics* 107.3 (Feb. 2022), pp. 1801–1817. ISSN: 1573-269X. DOI: 10.1007/s11071-021-07118-3. URL: <https://doi.org/10.1007/s11071-021-07118-3> (visited on 09/04/2025).

[28] Chia-Ying Lee et al. “An Environmentally Forced Tropical Cyclone Hazard Model”. en. In: *Journal of Advances in Modeling Earth Systems* 10.1 (2018). \_eprint: <https://onlinelibrary.wiley.com/doi/pdf/10.1002/2017MS001186>, pp. 223–241. ISSN: 1942-2466. DOI: 10.1002/2017MS001186. URL: <https://onlinelibrary.wiley.com/doi/abs/10.1002/2017MS001186> (visited on 05/27/2025).

[29] Chia-Ying Lee et al. “Autoregressive Modeling for Tropical Cyclone Intensity Climatology”. EN. In: *Journal of Climate* 29.21 (Nov. 2016). Publisher: American Meteorological Society Section: Journal of Climate, pp. 7815–7830. ISSN: 0894-8755, 1520-0442. DOI: 10.1175/JCLI-D-15-0909.1. URL: <https://journals.ametsoc.org/view/journals/clim/29/21/jcli-d-15-0909.1.xml> (visited on 11/02/2025).

[30] Chia-Ying Lee et al. “Rapid intensification and the bimodal distribution of tropical cyclone intensity”. en. In: *Nature Communications* 7.1 (Feb. 2016). Publisher: Nature Publishing Group, p. 10625. ISSN: 2041-1723. DOI: 10.1038/ncomms10625. URL: <https://www.nature.com/articles/ncomms10625> (visited on 06/06/2025).

[31] Jonathan Lin et al. “An Open-Source, Physics-Based, Tropical Cyclone Downscaling Model With Intensity-Dependent Steering”. en. In: *Journal of Advances in Modeling Earth Systems* 15.11 (2023). \_eprint: <https://onlinelibrary.wiley.com/doi/pdf/10.1029/2023MS003686>. ISSN: 1942-2466. DOI: 10.1029/2023MS003686. URL: <https://onlinelibrary.wiley.com/doi/abs/10.1029/2023MS003686> (visited on 10/31/2024).

[32] Jonathan Lin et al. “The response of tropical cyclone hazard to natural and forced patterns of warming”. en. In: *npj Climate and Atmospheric Science* 8.1 (Mar. 2025). Publisher: Nature Publishing Group, p. 109. ISSN: 2397-3722. DOI: 10.1038/s41612-025-00997-y. URL: <https://www.nature.com/articles/s41612-025-00997-y> (visited on 06/19/2025).

[33] Lasse Makkonen. “Plotting Positions in Extreme Value Analysis”. EN. In: *Journal of Applied Meteorology and Climatology* 45.2 (Feb. 2006). Publisher: American Meteorological Society Section: Journal of Applied Meteorology and Climatology, pp. 334–340. ISSN: 1558-8424, 1558-8432. DOI: 10.1175/JAM2349.1. URL: <https://journals.ametsoc.org/view/journals/apme/45/2/jam2349.1.xml> (visited on 11/25/2025).

[34] S.G. Mallat and Zhifeng Zhang. “Matching pursuits with time-frequency dictionaries”. In: *IEEE Transactions on Signal Processing* 41.12 (Dec. 1993), pp. 3397–3415. ISSN: 1941-0476. DOI: 10.1109/78.258082. URL: <https://ieeexplore.ieee.org/document/258082> (visited on 08/26/2025).

[35] Simona Meiler et al. “Intercomparison of regional loss estimates from global synthetic tropical cyclone models”. en. In: *Nature Communications* 13.1 (Oct. 2022), p. 6156. ISSN: 2041-1723. DOI: 10.1038/s41467-022-33918-1. URL: <https://www.nature.com/articles/s41467-022-33918-1> (visited on 12/17/2025).

[36] Andrew Mercer and Alexandria Grimes. “Atlantic Tropical Cyclone Rapid Intensification Probabilistic Forecasts from an Ensemble of Machine Learning Methods”. In: *Procedia Computer Science*. Complex Adaptive Systems Conference with Theme: Engineering Cyber Physical Systems, CAS October 30 – November 1, 2017, Chicago, Illinois, USA 114 (Jan. 2017), pp. 333–340. ISSN: 1877-0509. DOI: 10.1016/j.procs.2017.09.036. URL: <https://www.sciencedirect.com/science/article/pii/S1877050917318306> (visited on 04/19/2024).

[37] Daniel A. Messenger and David M. Bortz. “Weak SINDy: Galerkin-Based Data-Driven Model Selection”. In: *Multiscale Modeling & Simulation* 19.3 (Jan. 2021). arXiv:2005.04339 [math], pp. 1474–1497. ISSN: 1540-3459, 1540-3467. DOI: 10.1137/20M1343166. URL: <http://arxiv.org/abs/2005.04339> (visited on 09/12/2025).

[38] Hal F. Needham, Barry D. Keim, and David Sathiaraj. “A review of tropical cyclone-generated storm surges: Global data sources, observations, and impacts”. en. In: *Reviews of Geophysics* 53.2 (2015). \_eprint: <https://agupubs.onlinelibrary.wiley.com/doi/abs/10.1002/2014RG000477>. URL: <https://onlinelibrary.wiley.com/doi/abs/10.1002/2014RG000477> (visited on 12/18/2025).

[39] Jaideep Pathak et al. *FourCastNet: A Global Data-driven High-resolution Weather Model using Adaptive Fourier Neural Operators*. arXiv:2202.11214 [physics]. Feb. 2022. DOI: 10.48550/arXiv.2202.11214. URL: <http://arxiv.org/abs/2202.11214> (visited on 04/24/2025).

[40] P. Peduzzi et al. “Global trends in tropical cyclone risk”. en. In: *Nature Climate Change* 2.4 (Apr. 2012). Publisher: Nature Publishing Group, pp. 289–294. ISSN: 1758-6798. DOI: 10.1038/nclimate1410. URL: <https://www.nature.com/articles/nclimate1410> (visited on 05/10/2025).

[41] Jiangchao Qiu, Sai Ravela, and Kerry Emanuel. “From decades to years: Rising seas and cyclones amplify Bangladesh’s storm-tide hazards in a warming climate”. English. In: *One Earth* 8.4 (Apr. 2025). Publisher: Elsevier. ISSN: 2590-3330, 2590-3322. DOI: 10.1016/j.oneear.2025.101273. URL: [https://www.cell.com/one-earth/abstract/S2590-3322\(25\)00099-5](https://www.cell.com/one-earth/abstract/S2590-3322(25)00099-5) (visited on 11/20/2025).

[42] Michael Roth et al. “The Ensemble Kalman filter: a signal processing perspective”. In: *EURASIP Journal on Advances in Signal Processing* 2017.1 (Aug. 2017), p. 56. ISSN: 1687-6180. DOI: 10.1186/s13634-017-0492-x. URL: <https://doi.org/10.1186/s13634-017-0492-x> (visited on 06/21/2025).

[43] Lars R. Schade and Kerry A. Emanuel. “The Ocean’s Effect on the Intensity of Tropical Cyclones: Results from a Simple Coupled Atmosphere–Ocean Model”. EN. In: *Journal of the Atmospheric Sciences* 56.4 (Feb. 1999). Publisher: American Meteorological Society Section: Journal of the Atmospheric Sciences, pp. 642–651. ISSN: 0022-4928, 1520-0469. DOI: 10.1175/1520-0469(1999)056<0642:TOSEOT>2.0.CO;2. URL: [https://journals.ametsoc.org/view/journals/atsc/56/4/1520-0469\\_1999\\_056\\_0642\\_toseot\\_2.0.co\\_2.xml](https://journals.ametsoc.org/view/journals/atsc/56/4/1520-0469_1999_056_0642_toseot_2.0.co_2.xml) (visited on 11/20/2025).

[44] Hayden Schaeffer and Scott G. McCalla. “Sparse model selection via integral terms”. In: *Physical Review E* 96.2 (Aug. 2017). Publisher: American Physical Society, p. 023302. DOI: 10.1103/PhysRevE.96.023302. URL: <https://link.aps.org/doi/10.1103/PhysRevE.96.023302> (visited on 01/15/2025).

[45] Katherine Slyman et al. *Tipping in a Low-Dimensional Model of a Tropical Cyclone*. arXiv:2307.15583 [math]. July 2023. DOI: 10.48550/arXiv.2307.15583. URL: <http://arxiv.org/abs/2307.15583> (visited on 11/05/2025).

[46] Brian Tang and Kerry Emanuel. “A Ventilation Index for Tropical Cyclones”. en. In: (Dec. 2012). Section: Bulletin of the American Meteorological Society. DOI: 10.1175/BAMS-D-11-00165.1. URL: <https://journals.ametsoc.org/view/journals/bams/93/12/bams-d-11-00165.1.xml> (visited on 09/10/2025).

[47] Brian Tang and Kerry Emanuel. “Sensitivity of Tropical Cyclone Intensity to Ventilation in an Axisymmetric Model”. en. In: (Aug. 2012). Section: Journal of the Atmospheric Sciences. DOI: 10.1175/JAS-D-11-0232.1. URL: <https://journals.ametsoc.org/view/journals/atsc/69/8/jas-d-11-0232.1.xml> (visited on 08/20/2025).

[48] Margaret Trautner, Gabriel Margolis, and Sai Ravela. *Informative Neural Ensemble Kalman Learning*. arXiv:2008.09915 [cs]. Aug. 2020. DOI: 10.48550/arXiv.2008.09915. URL: <http://arxiv.org/abs/2008.09915> (visited on 10/27/2025).

[49] H. E. Willoughby, J. A. Clos, and M. G. Shoreibah. “Concentric Eye Walls, Secondary Wind Maxima, and The Evolution of the Hurricane vortex”. EN. In: *Journal of the Atmospheric Sciences* 39.2 (Feb. 1982). Publisher: American Meteorological Society Section: Journal of the Atmospheric Sciences, pp. 395–411. ISSN: 0022-4928, 1520-0469. DOI: 10.1175/1520-0469(1982)039<0395:CEWSWM>2.0.CO;2. URL: [https://journals.ametsoc.org/view/journals/atsc/39/2/1520-0469\\_1982\\_039\\_0395\\_cewswm\\_2\\_0\\_co\\_2.xml](https://journals.ametsoc.org/view/journals/atsc/39/2/1520-0469_1982_039_0395_cewswm_2_0_co_2.xml) (visited on 12/18/2025).

[50] Qidong Yang, Chia-Ying Lee, and Michael K. Tippett. “A Long Short-Term Memory Model for Global Rapid Intensification Prediction”. en. In: (Aug. 2020). Section: Weather and Forecasting. DOI: 10.1175/WAF-D-19-0199.1. URL: <https://journals.ametsoc.org/view/journals/wefo/35/4/wafD190199.xml> (visited on 06/30/2025).

[51] Zhihua Zeng, Lianshou Chen, and Yuqing Wang. “An Observational Study of Environmental Dynamical Control of Tropical Cyclone Intensity in the Atlantic”. en. In: *Monthly Weather Review* 136.9 (Sept. 2008), pp. 3307–3322. ISSN: 1520-0493, 0027-0644. DOI: 10.1175/2008MWR2388.1. URL: <http://journals.ametsoc.org/doi/10.1175/2008MWR2388.1> (visited on 12/04/2025).

[52] Fuqing Zhang and Dandan Tao. “Effects of Vertical Wind Shear on the Predictability of Tropical Cyclones”. en. In: (Mar. 2013). Section: Journal of the Atmospheric Sciences. DOI: 10.1175/JAS-D-12-0133.1. URL: <https://journals.ametsoc.org/view/journals/atsc/70/3/jas-d-12-0133.1.xml> (visited on 09/13/2025).

[53] Junxian Zhu et al. “A polynomial algorithm for best-subset selection problem”. In: *Proceedings of the National Academy of Sciences* 117.52 (Dec. 2020). Publisher: Proceedings of the National Academy of Sciences, pp. 33117–33123. DOI: 10.1073/pnas.2014241117. URL: <https://www.pnas.org/doi/10.1073/pnas.2014241117> (visited on 05/02/2025).